



# Investigation on Cold Formed Steel Channel Section with Curved Flanges Subjected to Axial Compression

S Arthi<sup>1</sup>(✉), D Suji<sup>1</sup>, and M Anbarasu<sup>2</sup>

<sup>1</sup> PSG College of Technology, Coimbatore, India  
arthisukumar7@gmail.com, dsu.civil@psgtech.ac.in

<sup>2</sup> Government college of Engineering, Salem, India

**Abstract.** In this study, the structural performance of cold-formed steel channel columns with curved flanges was numerically investigated. The elastic analysis was performed using CUFSM software. Both conventional and modified channel sections (curved flanges) were analyzed using ABAQUS, followed by validation of Channel Sections chosen from three different literatures; six samples from Ye et al. (2018a, 2018b), one from Anbarasu (2017) and one Semi Oval Hollow Cross Section proposed by Chen et al. (2018) with different yield stresses, under axial compression with pinned support conditions. The nonlinear stress-strain behaviour of the material and geometrical imperfections was incorporated to study these numerical models. Nominal Strength Design method using American Iron and Steel Institute, AISI-S100–16 and Allowable Stress Design using Indian Standard Code, IS 801–1975 were used to predict the axial strength of the compression members. An empirical equation derived by Parks et al. (1986) using nonlinear, least squares regression analysis for stub columns with unstiffened curved flanges that fail by elastic, local buckling was incorporated in the IS 801–1975 design procedure. The numerical parametric results from ABAQUS and the nominal strength predicted by the standard codal specifications are compared and discussed.

**Keywords:** Cold-formed steel · Buckling · Curved flange · Distortional · Nonlinear · Unstiffened

## 1 Introduction

Steel is the backbone of industries and the basic ingredient for growth and development of a country. Cold Formed Steel (CFS) sections are light-weight structural members that are formed by bending flat plane steel sheets or panels into various shapes at room temperature, and can be used to satisfy structural and functional requirements. Cold-formed steel provides a nearly 20% increase in strength over hot-rolled steel due to the usage of strain hardening. Furthermore, because the procedure is carried out at room temperature, the steel does not shrink as it cools, as it does in the hot-rolled method.

Bleich (1952) described that, by assuming that the flange-lip combination is undistorted and rotates around the flange-web junction, the distortional buckling strength is calculated. The longitudinal compressive stress acting on the web is anticipated to partially destabilize it and give elastic rotational and lateral restrictions to the flange at the flange-web interface. Where as in case of curved elements, the bent elements delay the failure due to local buckling. When out-of-plane deformation begins, they support each other by creating in-plane stiffness (arching action). They can be considered as an evolution in the stiffening of thin plate elements. Parks et al. (1986) used short stub column test results to evaluate the local buckling of both stiffened and unstiffened curved elements. On the basis of the classical energy technique, they established equations to estimate the buckling stresses of stiffened and unstiffened curved elements. By conducting a series of compression tests on a lipped channel section with and without intermediate stiffeners in the web, Kwon and Hancock (1992) developed two design curves, which were later adopted in the Effective Width Method (EWM) and Direct Strength Method (DSM), respectively. Schafer (2002) found that in the distortional mode, post buckling capacity is lesser than in the local mode, based on numerical calculations and testing. And presented a new design formulation that explicitly takes into account Local, Distortional, and Euler buckling. Zhu and Young (2011) investigated the cold-formed steel oval hollow sections under axial compression. The analysis showed that local buckling resistance of curved plate-in this case semi-circle was higher than that of the flats. Alireza et al. (2012) investigated on ductile moment-resisting frames (MRF) using cold-formed steel sections. The author had increased the ductility of the MRF by the introduction of curved flanges and stiffeners. Ye et al. (2016) studied the efficiency of the folded-flange beam section and concluded that the cross-section capacity of CFS beam sections is much influenced by providing edge stiffeners than intermediate web stiffeners in tge beam sections. Anbarasu (2017) studied the behaviour of specimen subjected to the most important and critical failure mode-combination of distortional and local buckling leading to modification of available design approach to suite for the combination of failure modes. Anil Kumar and Kalyanaraman (2018) provided a simple and accurate interaction design equation for CFS lipped channel compression members that provides for interaction between all potential buckling failure modes. Both experimental and numerical findings were used to validate the proposed interaction design equation. Chen and Young (2018) conducted a comprehensive investigation on CFS semi-oval hollow section columns. The semi-oval hollow sections investigated in this study were composed of one semi-circular flange, one flat flange and two flat web plates. Ye et al. (2018a, 2018b) conducted a study on buckling interaction in CFS channels under axial compression. Test results were used to verify the effectiveness of the Eurocode 3 design procedures. Ye et al. (2018a, 2018b) developed detailed non-linear FE models and validated with the tests on CFS columns. The Effective Width Method (EC3) and Direct Strength Method (DSM) were assessed with the validated FE models.

The recent studies demonstrated that CFS lipped channel sections with curved flanges possess high stiffness, strength and ductility compared to standard lipped channels. It is the only cross section with zero warping and has good torsional resistance, hence the failure will be only due to local and flexural buckling. It is easy to fabricate and also cost effective. Curved elements make up a large number of structural components,

either partially or entirely. Because they are frequently utilized and little is known about their structural behaviour, the current study was attempted to develop better analysis and design processes. Although there have been numerous studies on the buckling of curved elements under flexure, there have been few investigations on thin walled CFS columns with curved elements. As a result, the focus of this work is on the buckling of lipped channel sections with curved flanges when they are compressed.

## 2 Finite Element Modelling

To propose a Finite Element Modelling approach using ABAQUS v.6.11 software and to validate it, the column test results reported by Ye et al. (2018a, 2018b), Anbarasu (2017) and Chen et al. (2018) were considered. Accordingly, A and B series specimens were chosen from Ye where in A series represent the conventional Channel cross sections available in markets with varying lengths-1000 mm, 1500 mm and 2000 mm. Similarly, B series specimens are the optimized Channel cross sections as suggested by Ye et al. (2018a, 2018b). Further one more cross section of a Channel was chosen from the literature reported by Anbarasu (2017). Since the proposed model for this project is new, a similar specimen having Semi Oval Hollow Section reported by Chen et al. (2018) was also chosen for the validation of Curved Flanges.

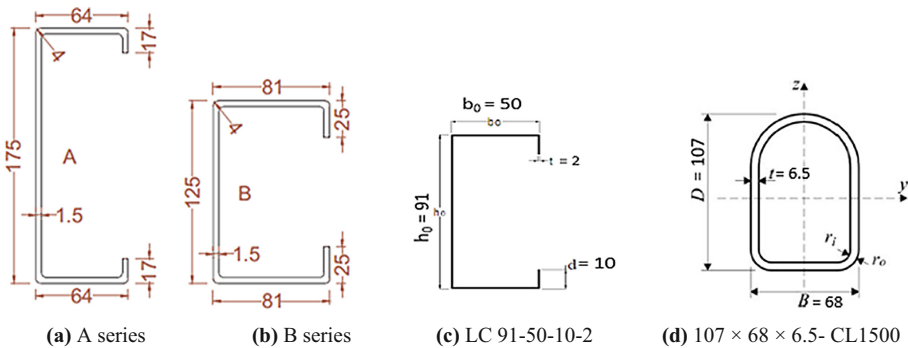


**Fig. 1.** Specifications of models chosen from the literatures.

A pictorial representation of the chosen models from the previously said literatures are shown in Fig. 1. The cross section centerline dimensions were used to create the finite element models. The geometric centroid of the segment was used to establish reference points. To simulate the pinned support conditions, rigid body tie constraints were applied by following Anbarasu and Ashraf (2019). A 4 node doubly curved thin shell, reduced integration, hourglass control, using five degrees of freedom per node - S4R5 was used in FE modelling. Hinged boundary condition was achieved by restraining  $U_x$ ,  $U_y$ ,  $U_z$  and  $\theta_z$  at the unloaded end and restraining  $U_x$ ,  $U_z$  and  $\theta_z$  at the loaded end. Following the linear Eigen buckling analysis, a non-linear buckling analysis was performed, in which material non-linearity was included in the FE model. For lipped channels, the overall imperfection was taken as 1/1000 of the complete length of the column at the mid-height

segment (Camotim et al. 2011) along with local imperfection magnitude of 0.34t. The adopted FE modelling approach was validated against the tests reported by Ye et al. (2018a, 2018b), Anbarasu (2017) and Chen et al. (2018). The specimen identifications were named as given in that particular literature.

The chosen models were then validated using FE Modelling. The buckling modes obtained from the FE analysis are compared with the experimental buckling modes obtained from that particular literatures which are shown in Fig. 2 wherein the failure modes obtained from the FEM matches with the experimental work. The Load vs Axial Deformation charts for the validated models are shown in Fig. 3. The capacities of the models chosen are tabulated in Table 1 which shows that the FEM predicted axial compressive strength ( $P_{FEM}$ ) for validated columns agrees to the experimental results ( $P_{EXP}$ ), with a mean of 0.98 and a standard deviation of 0.04 thereby concluding that the FE modelling procedure is validated. After validation, same procedure was adopted for the analysis of proposed CCF models.

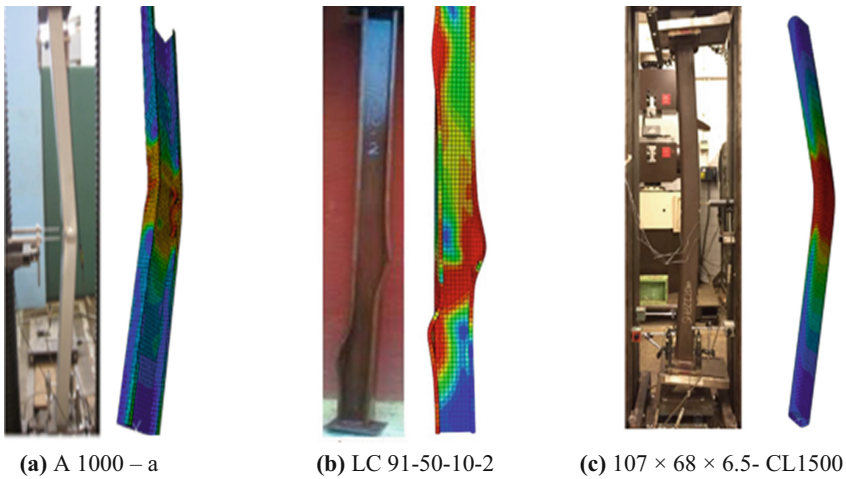
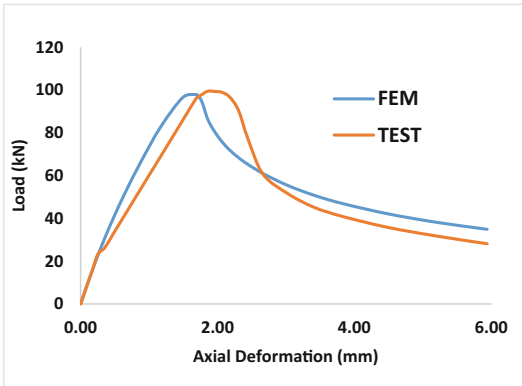


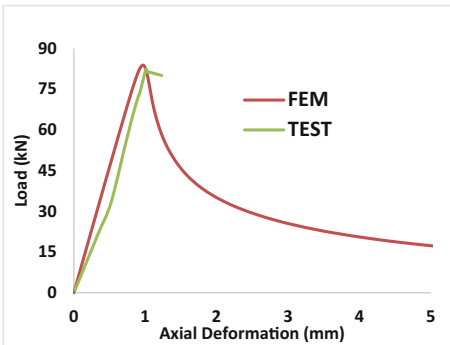
**Fig. 2.** Validation results.

**Table 1.** Validation results of standard models chosen

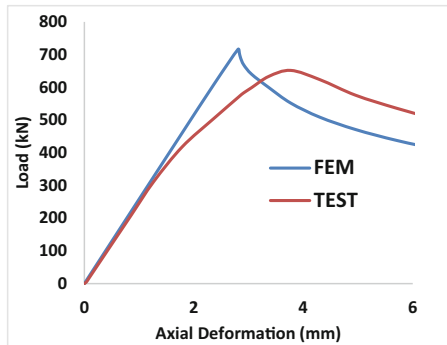
Sl	Identification	Area (mm <sup>2</sup> )	$P_{EXP}$ (kN)	$P_{FEM}$ (kN)	$\frac{PEXP}{PFEM}$
1	<b>A1000-a</b>	485.18	98.93	97.92	1.01
2	<b>B1000-b</b>	486.24	110.30	114.00	1.03
3	<b>A1500-b</b>	480.31	85.30	83.70	0.98
4	<b>B1500-b</b>	491.79	107.90	103.70	0.96
5	<b>A2000-b</b>	489.51	75.80	78.39	1.03
6	<b>B2000-c</b>	489.13	105.30	101.32	0.96
7	<b>LC 91-50-10-2</b>	406	82.20	83.76	0.98
8	<b>107 × 68 × 6.5-CL1500</b>	1861.1	660.8	716.18	0.92
<b>Mean</b>					0.98
<b>Standard Deviation</b>					0.04



(a) A 1000 – a



(b) LC 91-50-10-2



(c) 107 × 68 × 6.5- CL1500

**Fig. 3.** Comparison of test and FEM results.

### 3 Specimen Geometry

A parametric study was carried out on validated models to propose a Channel with Curved Flange to eliminate the distortional buckling.

1. Two sets of channels with curved flanges are proposed; Set - I and Set - II.
2. Set - I models are the ones derived from A and B series models reported by Ye et al. (2018a, 2018b). The models were considered for the lengths 1000 mm, 1500 mm and 2000 mm with a thickness of 1.5 mm and modelled for the yield stress of  $447 \text{ N/mm}^2$  and ultimate stress of  $550 \text{ N/mm}^2$  with a Young's modulus of  $2 \times 10^5 \text{ N/mm}^2$ .
3. Whereas Set - II models are the ones derived based on LC 91–50–10–2 model suggested by Anbarasu (2017). The models were considered for a length of 876 mm with a thickness of 1.5 mm and modelled for the yield stress of  $268 \text{ N/mm}^2$  and ultimate stress of  $315 \text{ N/mm}^2$  with a Young's modulus of  $2 \times 10^5 \text{ N/mm}^2$ .
4. The overall depth of the proposed models are made sure such that it approximately matches with the validated models chosen, i.e., Sum of the web depth and radius of flanges approximately equals the web depth of validated models.
5. Not only the overall depth but also the cross sectional area is taken into account for the proposal of new models.

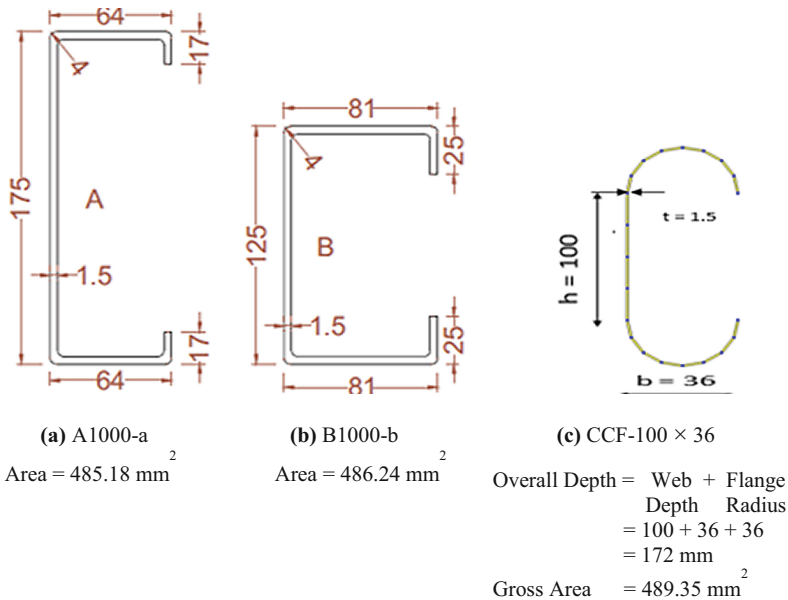
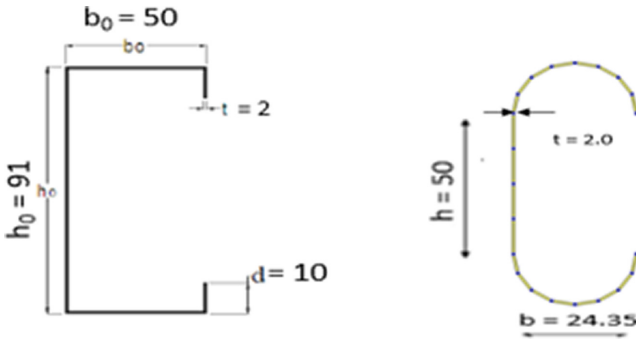


**Fig. 4.** Set – I.

The cross sectional dimensions and their respective area of series A and B listed under Set - I are shown in Fig. 4(a) and Fig. 4(b). The Fig. 4(c) shows the dimensions of the model proposed along with the explanation for the arrival of gross sectional area



(a) LC 91-50-10-2

$$A = 406 \text{ mm}^2$$

(b) CCF-60 × 22.8

$$\begin{aligned} \text{Overall Depth} &= \text{Web Depth} + \text{Flange Radius} \\ &= 50 + 24.35 + 24.35 \\ &= 98.7 \text{ mm} \\ \text{Gross Area} &= 406.85 \text{ mm}^2 \end{aligned}$$

Fig. 5. Set – II.

which almost matches with the base models. Similarly the models for Set - II are also proposed which is explained in Fig. 5. Therefore on this basis a total of 8 possible models for Set - I and 4 models for Set - II are obtained. Their geometric properties are listed in Table 2. The models were named based on their cross sectional geometry and dimensions. Therefore, in the specimen identification, CCF stands for Channel with Curved Flange followed by the web depth and flange radius; CCF-125 × 25.

### 4 Design Methods

Nominal Strength Design method using American Iron and Steel Institute, AISI-S100–16 and Allowable Stress Design using Indian Standard Code, IS 801–1975 were adopted for the determination of compressive strength of members. To determine  $Q$ , the ratio between the allowable compressive stress and basic design stress for members composed of unstiffened elements, in this case - the curved elements (curved flange), the expression (Eq. 1) presented by Parks et al. (1986) was considered.

$$f_{cr} = \left( 0.04068 \frac{t}{R} + 0.45192 \left( \frac{t}{b} \right)^2 \right) E \tag{1}$$

where  $f_{cr}$  is the elastic buckling stress of unstiffened curved element with a thickness  $t$ , radius of curvature  $R$ , arc length  $b$  and Young’s Modulus  $E$ .

For comparing the design strengths obtained from the two different design approaches, the Load and Resistance Factor Design (LRFD) value obtained from AISI

**Table 2.** Geometric properties of the proposed models

Sl	Group	Identification	Web depth (mm)	Flange radius (mm)	Cross sectional area (mm <sup>2</sup> )
1	Set - I	CCF-125 × 25	125	25	423.34
2	Set - I	CCF-100 × 30	100	30	432.89
3	Set - I	CCF-100 × 35	100	35	479.94
4	Set - I	CCF-105 × 35	105	35	487.44
5	Set - I	CCF-100 × 36	100	36	489.35
6	Set - I	CCF-117 × 33	117	33	492.02
7	Set - I	CCF-130 × 32	130	32	496.6
8	Set - I	CCF-100 × 37.5	100	37.5	503.46
9	Set - II	CCF-50 × 24.35	50	24.35	406.3
10	Set - II	CCF-60 × 22.8	60	22.8	406.85
11	Set - II	CCF-70 × 21.2	70	21.2	406.78
12	Set - II	CCF-50 × 20	50	20	351.72

approach was considered. The *LRFD* value was obtained by multiplying the nominal strength by a factor 0.85. As the Design Strength obtained from IS Method was already available in allowable state, the value was taken directly for comparison. As FEM provides factored design strength, the value was divided by the material safety factor (1.15) to obtain the allowable design strengths. The Design Strengths were calculated in terms of stresses and the ratio of  $\frac{\sigma_{FEM}}{\sigma_{LRFD}}$  (AISI) and  $\frac{\sigma_{FEM}}{\sigma_{al}}$  (IS) for both the sets are tabulated in Table 3, wherein  $\sigma_{FEM}$  is the stress obtained from Finite Element Modelling,  $\sigma_{LRFD}$  is the stress obtained from AISI approach and  $\sigma_{al}$  is the stress obtained from IS approach.

The mean value for the ratio  $\frac{\sigma_{FEM}}{\sigma_{LRFD}}$  (AISI) is found to be 0.95 with a standard deviation of 0.08 and mean for ratio  $\frac{\sigma_{FEM}}{\sigma_{al}}$  (IS) is found to be 1.05 with a standard deviation of 0.15.

The Load vs Axial Deformation curves for Set - I models having lengths 1000 mm, 1500 mm and 2000 mm are shown in Fig. 6, Fig. 7 and Fig. 8. The FEM visualization of the proposed model CCF-100 × 36 is shown in Fig. 9. The figures clearly show that the failure is caused due to Local and Flexural modes only. Similarly the Load vs Axial Deformation curve for Set - II models having length 876 mm is shown in Fig. 10 and the FEM visualization of the proposed model CCF-50 × 24.35 is shown in Fig. 11 which also shows that the failure is caused due to Local and Flexural modes only.



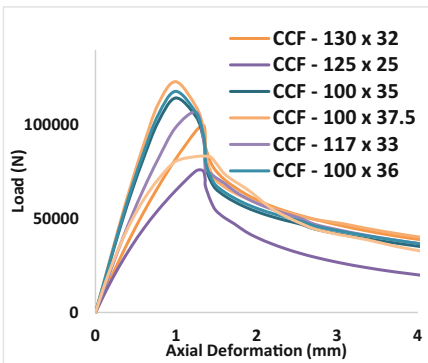
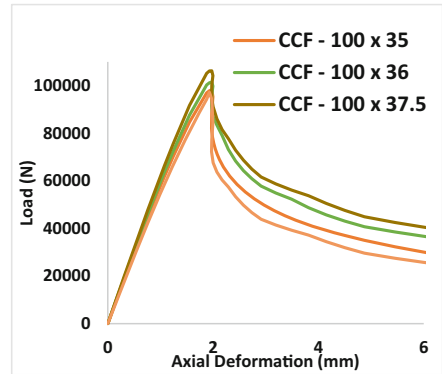
**Table 3.** Comparison of FEM, AISI and IS results for CCF models

Sl	Identification	Length (mm)	$\sigma_{FEM}$ N/mm <sup>2</sup>	$\sigma_{LRFD}$ (AISI) N/mm <sup>2</sup>	$\sigma_{al}$ (IS) N/mm <sup>2</sup>	$\frac{\sigma_{FEM}}{\sigma_{LRFD}}$ (AISI)	$\frac{\sigma_{FEM}}{\sigma_{al}}$ (IS)
1	<b>CCF-125 x 25</b>	1000	155.16	199.17	195.18	0.78	0.79
2	<b>CCF-100 x 30</b>	1000	200.35	207.54	215.82	0.97	0.93
3	<b>CCF-100 x 35</b>	1000	207.1	208.62	209.35	0.99	0.99
4	<b>CCF-105 x 35</b>	1000	200.24	202.04	208.76	0.99	0.96
5	<b>CCF-100 x 36</b>	1000	209.43	208.19	209.17	1.01	1.00
6	<b>CCF-117 x 33</b>	1000	188.73	189.64	208.71	1.00	0.90
7	<b>CCF-130 x 32</b>	1000	174.77	178.13	207.87	0.98	0.84
8	<b>CCF-100 x 37.5</b>	1000	212.47	209.19	210.58	1.02	1.01
9	<b>CCF-100 x 30</b>	1500	167.44	177.7	194.2	0.94	0.86
10	<b>CCF-100 x 35</b>	1500	178.06	181.65	179.79	0.98	0.99
11	<b>CCF-105 x 35</b>	1500	173.5	175.36	178.44	0.99	0.97
12	<b>CCF-100 x 36</b>	1500	180.39	181.08	179.36	1.00	1.01
13	<b>CCF-117 x 33</b>	1500	162.23	164.7	178.36	0.99	0.91
14	<b>CCF-100 x 37.5</b>	1500	183.47	183.4	182.43	1.00	1.01
15	<b>CCF-100 x 35</b>	2000	145.77	146.53	134.37	1.00	1.08
16	<b>CCF-100 x 36</b>	2000	149.5	149.12	138.28	1.01	0.92
17	<b>CCF-50 x 24.35</b>	876	169.56	187.62	123.69	0.90	1.37
18	<b>CCF-60 x 22.8</b>	876	159.03	187.63	123.7	0.85	1.29

*(continued)*

**Table 3.** (continued)

Sl	Identification	Length (mm)	$\sigma_{FEM}$ N/mm <sup>2</sup>	$\sigma_{LRFD}$ (AISI) N/mm <sup>2</sup>	$\sigma_{al}$ (IS) N/mm <sup>2</sup>	$\frac{\sigma_{FEM}}{\sigma_{LRFD}}$ (AISI)	$\frac{\sigma_{FEM}}{\sigma_{al}}$ (IS)
19	<b>CCF-70 x 21.2</b>	876	148.35	186.72	123.29	0.79	1.20
20	<b>CCF-50 x 20</b>	876	144.35	177.34	119.17	0.81	1.21
<b>Mean</b>						0.95	1.02
<b>Standard Deviation</b>						0.08	0.15

**Fig. 6.** Load vs Axial deformation for L = 1000 mm.**Fig. 7.** Load vs Axial deformation for L = 1500 mm.

## 5 Discussion on Results

From the results, it was evident that the proposed models showed better performances than the standard channel.

### 5.1 Discussion on FEM Results

The performances of models for length 1000 mm given in Table 4 are discussed below:

The Model CCF-125 × 25 showed poor performance than the standards. But models, CCF-100 × 30 and CCF-100 × 35 exhibited greater strength even though it had minimum cross sectional area than the standards. Also models, CCF-105 × 35 and CCF-100 × 36 exhibited greater strength with almost equivalent cross sectional area. Further models CCF-117 × 33, CCF-130 × 32 and CCF-100 × 37.5 had very large cross sectional area and exhibited higher strengths.

The Set - I models were further analyzed for the lengths 1500 mm and 2000 mm and their performances are discussed below:

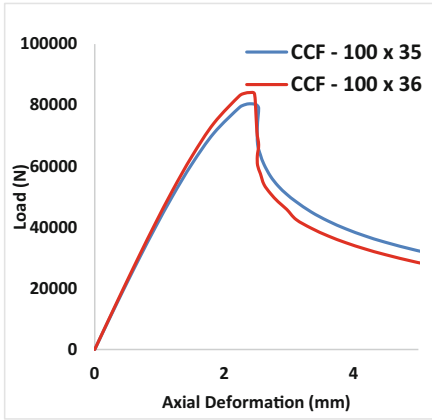


**Fig. 8.** Load vs Axial deformation for  $L = 2000$  mm.

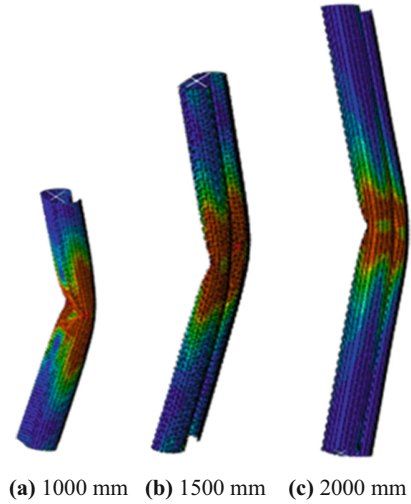


**Fig. 9.** FEM result for CCF-100  $\times$  36.

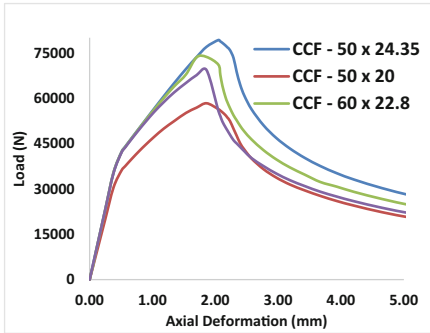


**Fig. 10.** Load vs Axial deformation for  $L = 876$  mm.

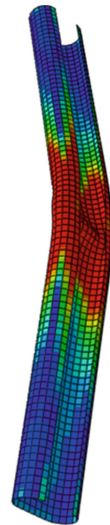


**Fig. 11.** FEM result for CCF-50  $\times$  24.35.

Although having lesser cross sectional areas, the Models CCF-100  $\times$  30 and CCF-100  $\times$  35 showed better performances for longer lengths as well. And the Models, CCF-105  $\times$  35, CCF-100  $\times$  36 and CCF-117  $\times$  33 again exhibited higher strengths.

From this interpretation, it can be concluded that the overall performance of Model CCF-100 × 35, although having lesser cross sectional area showed better performances for all ranges of lengths listed. And the Model CCF-100 × 36 exhibited greater strength with almost equivalent cross sectional area for all ranges of lengths listed.

In Table 5, the Set - II models were analyzed for the length 876 mm. From this analysis it can be concluded that the Model CCF-50 × 20 exhibited almost equivalent strength with minimum cross sectional area. And the Models CCF-50 × 24.35, CCF-70 × 21.2 and CCF-60 × 22.8 exhibited greater strength with almost equivalent cross sectional area.

Therefore from the results, it is understood that for the same cross sectional area, the performances of the models varies such that models with increase in radius of flange provides better results than the models with increase in depth of web. Also the influence of curved flanges is very much evident on the mode of failure; combination of Local and Flexural Buckling.

**Table 4.** FEM results for set - I models

S.No	Identification	Area (mm <sup>2</sup> )	Length (mm)	$P_{FEM}$ (kN)	Mode of Failure
1	<b>A1000-a</b>	485.18	1000	98.93	L + D
2	<b>B1000-b</b>	486.24	1000	110.3	L + D
3	<b>CCF-125 × 25</b>	423.34	1000	75.54	L + F
4	<b>CCF-100 × 30</b>	432.89	1000	99.75	L + F
5	<b>CCF-100 × 35</b>	479.94	1000	114.32	L + F
6	<b>CCF-105 × 35</b>	487.44	1000	112.26	L + F
7	<b>CCF-100 × 36</b>	489.35	1000	117.87	L + F
8	<b>CCF-117 × 33</b>	492.02	1000	106.79	L + F
9	<b>CCF-130 × 32</b>	496.6	1000	99.82	L + F
10	<b>CCF-100 × 37.5</b>	503.46	1000	123.03	L + F
11	<b>A1500-b</b>	480.31	1500	85.3	L + D
12	<b>B1500-b</b>	491.79	1500	107.9	L + D
13	<b>CCF-100 × 30</b>	432.89	1500	83.36	L + F
14	<b>CCF-100 × 35</b>	479.94	1500	98.29	L + F
15	<b>CCF-105 × 35</b>	487.44	1500	97.26	L + F
16	<b>CCF-100 × 36</b>	489.35	1500	101.52	L + F
17	<b>CCF-117 × 33</b>	492.02	1500	91.8	L + F

(continued)

**Table 4.** (continued)

S.No	Identification	Area (mm <sup>2</sup> )	Length (mm)	$P_{FEM}$ (kN)	Mode of Failure
18	<b>CCF-100 × 37.5</b>	503.46	1500	106.23	L + F
19	<b>A2000-b</b>	489.51	2000	75.80	L + D
20	<b>B2000-c</b>	489.13	2000	105.30	L + D
21	<b>CCF-100 × 35</b>	479.94	2000	80.46	L + F
22	<b>CCF-100 × 36</b>	489.35	2000	84.13	L + F

**Table 5.** FEM results for set - II models for length 876 mm

S.No	Identification	Area (mm <sup>2</sup> )	$P_{FEM}$ (kN)	Mode of Failure
1	<b>LC 91-50-10-2</b>	406	82.2	L + D
2	<b>CCF-50 × 20</b>	351.72	85.52	L + F
3	<b>CCF-50 × 24.35</b>	406.3	102.70	L + F
4	<b>CCF-70 × 21.2</b>	406.78	100.23	L + F
5	<b>CCF-60 × 22.8</b>	406.85	101.82	L + F

## 5.2 Discussion on Results from Design Methods

The explanation for deviation of results tabulated in the Table 3 can be explained as follows:

1. As a result of the expansion to wholly unique cross-sections, new or modified DSM and IS strength expressions may be required.
2. A design technique that accounts for the interaction of local and flexural buckling is required.
3. Because the codes do elastic buckling analysis for the entire cross-section rather than for individual elements, even if only a small area of the cross-section buckles, the codes will estimate a low strength for the entire member.

Therefore it can be concluded that both the design approaches are not conservative. Hence the codes must be revised before incorporating curved flanges.

## 6 Conclusions

The current study presents a numerical investigation of the response of pinned end cold-formed channel columns and curved flange channel section under compression.

- The nonlinear finite element modelling technique developed was validated and used for finding the load carrying capacity of models specified.

- FEM predicted that the compressive strength for channels with curved flange columns was better than the standard channel sections, hence these models can also be used wherever required.
- With the inclusion of expression given in Eq. 1, IS design procedure provides conservative results for most of the models, whereas AISI design procedure provides unconservative results.
- From the buckling shapes obtained from FEM results, it can be concluded that introduction of curved flange eliminates distortional buckling.
- And the failure of proposed models are mainly due to Local and Flexural failure modes.

The research shall be further verified with experimental work which is yet to be completed by the authors.

## References

- AISI: North American Specification for the Design of Cold-formed Steel Structural Members, 2016 Edition, AISI-S100-16, Washington, DC (2016)
- Anbarasu, M.: Influence on ultimate strength of cold formed steel lipped channel columns subjected to interaction on distortional - global buckling. *Adv. Nat. Appl. Sci.* **11**(8), 192–201 (2017). Article first published online: 6 Nov 2017
- Anbarasu, M., Ashraf, M.: Structural behavior of intermediate length cold-formed steel rack columns with C-stitches. *Front. Struct. Civ. Eng.* **13**(4), 937–949 (2019). <https://doi.org/10.1007/s11709-019-0528-4>
- Anil Kumar, M.V., Kalyanaraman, V.: Interaction of local, distortional, and global buckling in CFS lipped channel compression members. *J. Struct. Eng. (ASCE)* **144**(2), 04017192-1–9 (2018)
- Anonymous: I.S 801: Use of Cold Formed Light Gauge Steel Structural Members in General Building Construction. Indian Standard Institution, India (1975)
- Bleich, F.: *Buckling Strength of Metal Structures*. Mc-Graw Hill Book Co., Inc., New York (1952)
- Camotim, D., Dinis, P.B.: Coupled instabilities with distortional buckling in cold-formed steel lipped channel columns. *J. Thin-walled Struct.* **49**(5), 562–575 (2011)
- CEN: Eurocode 3: Design of Steel Structures, Part 1.3: General Rules — Supplementary Rules for Cold-formed Steel Members and Sheeting in Brussels: European Committee for Standardization (2005)
- Zhu, J.-H., Ben Young, M.: Cold-formed-steel oval hollow sections under axial compression. *J. Struct. Eng.* **137**, 719–727 (2011)
- Ye, J., Hajirasouliha, I., Becque, J.: Experimental investigation of local-flexural interactive buckling of cold formed steel channel columns. *J. Thin Walled Struct.* **125**, 245–258 (2018a)
- Ye, J., Hajirasouliha, I., Becque, J., Pilakoutas, K.: Development of more efficient cold-formed steel channel sections in bending. *J. Thin Walled Struct.* **101**, 1–13 (2016)
- Ye, J., Mojtabaei, S.M., Hajirasouliha, I.: Local-flexural interactive buckling of standard and optimised cold-formed steel columns. *J. Thin Walled Struct.* **144**, 106–118 (2018b)
- Kwon, Y.B., Hancock, G.J.: Tests of cold-formed channels with local and distortional buckling. *J. Struct. Eng. (ASCE)* **117**(7), 1786–1803 (1992)
- Chen, M.-T., Young, B.: Experimental and numerical investigation on cold-formed steel semi-oval hollow section compression members. *J. Constr. Steel Res.* **151**, 174–184 (2018)
- Parks, M.B., Santaputra, C., Yu, W.W.: Local Buckling of Curved Elements, Eighth International Specialty Conference on Cold-Formed Steel Structures, pp. 277–294. St. Louis, Missouri, U.S.A. (1986)

- Sabbagha, A.B., Petkovski, M., Pilakoutas, K., Mirghaderi, R.: Development of cold-formed steel elements for earthquake resistant moment frame buildings. *J. Thin Walled Struct.* **53**, 99–108 (2012)
- Schafer, B.W.: Local, distortional, and euler buckling of thin-walled columns. *J. Struct. Eng. (ASCE)* **128**(3), 289–299 (2002)